Korean J. Chem. Eng., 38(4), 862-871 (2021)
DOI: 10.1007/s11814-020-0691-2

pISSN: 0256-1115
eISSN: 1975-7220

Selective CO_2 adsorption using N-rich porous carbon derived from KOH-activated polyaniline

Soodabeh Khalili and Mohsen Jahanshahi†

Department of Chemical Engineering, Babol Noshirvani University of Technology, Shariati Av., Babol, P.O. Box: 484, 47148-71167, Iran

(*Received 3 August 2020 • Revised 26 September 2020 • Accepted 3 October 2020*)

Abstract−The adsorption of pure gases of carbon dioxide, methane and nitrogen was examined on nitrogen-doped porous carbon (NDC) prepared from polyaniline (PANI) as precursor by chemical activation with KOH (T=650°, IR=2, t=1 h) to determine the potential for the separation of CO_2 gas from flue gas or natural gas. Adsorption equilibrium of all gases was determined in a temperature range of 298-318 K and pressure up to 14 bar. Results demonstrated an excellent CO_2 adsorption capacity of 3.09 mmol·g^{-1} owing to high CO_2 interaction affinity with NDC surface compared to CH_4 (1.43 mmol·g^{-1}) and N_2 (0.64 mmol·g^{-1}) under ambient condition (298 K and 1 bar). The ideal adsorbed solution theory (IAST) was used to determine the adsorption selectivity of NDC for CO_2/CH_4 and CO_2/N_2 mixtures at different compositions. The NDC had CO_2/CH_4 (4.42 and 4.08 for CO_2/CH_4=10/90 and 50/50, respectively) and CO_2/N_2 (12.81 and 12.08 for CO_2/N_2=15/85 and 50/50, respectively) IAST selectivity at temperature of 298 K and pressure of 1bar. The moderate CO_2 adsorption enthalpy indicates that N-doped activated carbon is a promising material in gas separation such as natural gas and flue gas processing.

Keywords: Nitrogen-doped Porous Carbon, Gas Adsorption, Polyaniline, CO_2/CH_4 and CO_2/N_2, Selectivity

INTRODUCTION

Global warming and ocean acidification are among the consequences of increasing the carbon dioxide concentration in the atmosphere, especially in the recent century [1,2]. The flue gas generated from the combustion of fossil fuel in power plants is the primary source of CO_2 emission into the atmosphere. Therefore, to reduce anthropogenic CO_2 emissions in the atmosphere, CO_2 should be selectively separated from the flue gas [3,4]. Additionally, due to the rising global demand for energy and also less CO_2 emission, natural gas as a clean fuel has become a significant energy source in the daily life of people. Actually, biogas as well as landfill gas is categorized in methane-containing gases which can be alternatively used as clean fuels [5,6]. The presence of CO_2 as impurity in natural gas will cause pipeline and equipment corrosion and reduce gas quality, calorific values and also the volume of gas transported through cylinders and pipeline. Therefore, to improve the quality of gas, it is necessary to eliminate CO_2 from natural gas [7,8]. A handful of techniques for CO_2 removal from the natural gas or flue gas are amine absorption, cryogenic distillation, membrane and adsorption [9]. Among these diverse separation methods, adsorption by porous materials has been suggested as a practical and cost-efficient alternative because of its low cost, low energy consumption, easy handling and relatively high efficiency to conventional techniques in industry like amine absorption [10-13].

During recent years, porous solid adsorbents have been extensively explored for CO_2 separation [14-18]. Among these materials, porous carbons have attracted intense interest due to the high specific surface area, uniform and narrow pore size distribution, strong thermal stability, low energy consumption, the lower production cost and ease of regeneration [19,20]. Many studies have been made for improving the performance of carbon materials for selective CO_2 adsorption. In general, gas selectivity properties can be increased in two ways. First is by application of the molecular sieving effect by pore size distribution tuning in order to separate different gas molecules with different kinetic diameter [21]. Second strategy is to increase the surface polarity for improving the adsorption interaction due to the differences in electronic properties of molecules of gases [22]. Therefore, incorporation of N element into the carbon structure can obviously improve the electronic distribution of the carbon, which causes to increase CO_2 adsorption. Because CO_2 has higher quadruple moment than CH_4 and N_2, therefore strong interaction between CO_2 and N element of the surface occurs, which causes the selective elimination of CO_2 from the natural gas or flue gas [23,24].

In recent years, application of N-rich polymers such as polyacrylonitrile [25], polypyrrole [26] and PANI [27] has received much attention for synthesizing n doped-porous carbon adsorbents. Due to the large amount of nitrogen content, simple synthesis process and chemical stability, PANI has been considered as a suitable substance to synthesize nitrogen-containing porous carbon [28].

Physical and chemical activation techniques are often applied for preparation of porous carbons with high surface area and porosity. Physical activation takes place in two sequential steps: first step is pyrolization of the precursor materials at a medium-high temperature (300-800 °C) in an inert atmosphere to prepare char. The

†To whom correspondence should be addressed.
E-mail: mmohse@yahoo.com

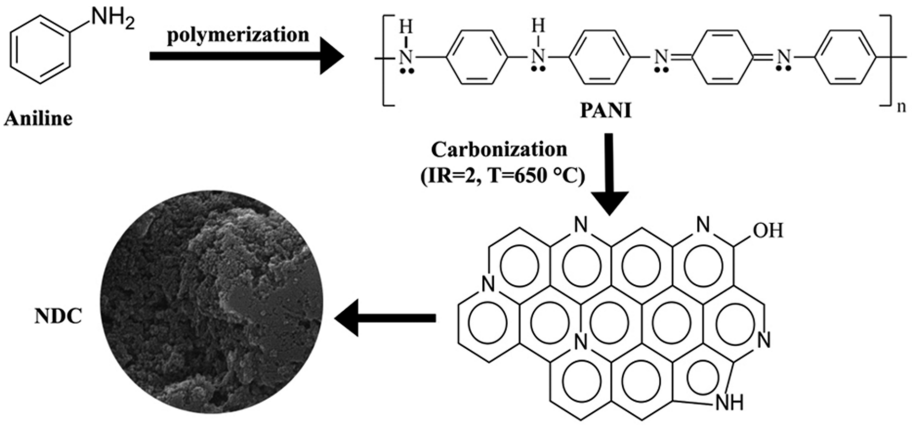

Fig. 1. Synthetic route of the NDC carbonized derivative from PANI.

second stage is activation of char at a higher temperature (700-1,000 °C) with a flow of steam or CO_2 gases. In chemical activation, the precursor is impregnated with chemicals such as KOH, H_3PO_4, K_2CO_3 or $ZnCl_2$ and carbonized at moderate temperatures (550 °C) in an inert atmosphere [29,30]. Among these, KOH activating agent is widely applied for preparation of porous carbonaceous materials due to the generation of adsorbents with high surface area and wide and narrow micropores on their surface which are important for increasing the CO_2 adsorption capacities [31]. To our knowledge, no studies have focused on the application of n doped porous carbon derived from PANI for selective removal of CO_2 from natural gas. The aim of this work was preparation of N-doped porous adsorbent by using PANI as an organic precursor and chemical activation method with KOH as an effective activation agent to construct highly porous carbon. Pure CO_2, CH_4 and N_2 adsorption equilibrium by the prepared adsorbent was evaluated volumetrically under different pressures up to 14 bar as well as different adsorption temperature (298-318 K). Also, the isotherm, CO_2/N_2 and CO_2/CH_4 selectivity and thermodynamic properties were studied to provide further insight about application of this prepared adsorbent in separation of CO_2 from flue gas or natural gas.

EXPERIMENTAL SECTION

1. Materials

Aniline (AR grade, Merck), sulfuric acid (98%, Scharlau), ammonium peroxydisulfate (Merck) and ethanol (Merck) were used for preparation of PANI as precursor. Potassium hydroxide (Scharlau) and hydrochloric acid (37%, Scharlau) were applied for synthesis of N-doped activated carbon. All chemicals used in this study were of analytical grade. All gases with high purity have been used in this study, which were carbon dioxide (99.998%), helium (99.995%), methane (99.995%) and nitrogen (99.995%).

2. Adsorbent Preparation

Before the preparation of polyaniline, aniline monomer was distilled twice to eliminate the oxidation impurities. 100 ml of H_2SO_4 solution (1 M) and 1 g of ammonium peroxydisulfate (APS) were mixed and stirred for 30 min at room temperature. Aniline (1 ml) was slowly added to H_2SO_4 and APS solution at room temperature and stirred under vigorous stirring for 5 h. Afterwards, the filtrated polymer was rinsed sequentially several times with distilled water and ethanol to remove impurities in the adsorbent and next heated in a vacuum oven for 24 h (60 °C.) The prepared polymer was used as precursor for the preparation of N-doped sorbent.

For construction of NDC, the dried material (PANI) was impregnated with KOH as an activation agent with impregnation ratio of 2 : 1 (the weight ratio of KOH to PANI) and stirred at 90 °C for 3 h. After mixing, the impregnated PANI was dried in the vacuum oven at 110 °C for 20 h. The prepared material then inserted in a tubular quartz glass reactor and heated in an electric furnace for 1 h at 650 °C under nitrogen gas with constant flow rate. After carbonization, the final product was dispersed in HCl solution (0.5 M) for 30 min to remove any impurity and open pores. Finally, the NDC was rinsed several times with distilled water until the pH value of the wash water showed neutral pH. The resulting adsorbent was collected and dried at 110 °C overnight for the following characterization and gas adsorption test. The preparation process for NDC is illustrated schematically in Fig. 1. The yield of prepared sorbent was defined as follows

$$\text{Yield} = \frac{w}{w_0} * 100 \quad (1)$$

where w(g) and w_0(g) are the final weight of NDC and the dry PANI, respectively.

3. Characterization Techniques

The pore structure and surface area of sorbent was done by nitrogen adsorption-desorption isotherm at 77 K using the Brunauer-Emmett-Teller (BET) method (BELsorp-miniII, BEL Inc., Japan). The mesopore size distribution was estimated by Barrett-Joyner-Halenda (BJH) method. Prior to analysis, the adsorbent was degassed at 373 K for 5 h. Scanning electron microscopy (SEM) using an EGA II LMU, Tescan, Czech Republic microscope was applied to assess the morphology of the prepared PANI and NDC. FTIR spectra of the prepared materials were recorded by Bruker Vertex-70 infrared spectrometer using KBr disks as reference sample with the wavenumber range of 4,000-400 cm^{-1}. CHNS elemental analysis of synthesized materials was performed with an elemental analyzer (Costech ECS 4010, Italy).

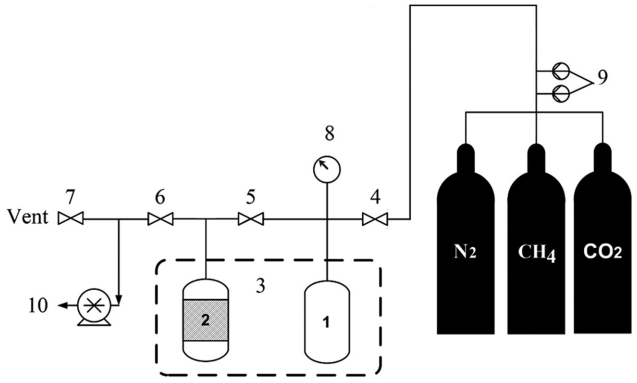

Fig. 2. Apparatus used for experimental study of pure gases adsorption.

1. Reference cell
2. Adsorbent cell
3. Water bath
4-7. Valves
8. Pressure digital indicator
9. Regulator
10. Vacuum pump

4. Experimental Set-up

The adsorption isotherms of pure gases were determined using a static volumetric apparatus depicted in Fig. 2. The experimental setup basically consists of a reference cell for gas storage and adsorbent cell and is held in a water bath to keep the temperature of the adsorption process constant during the adsorption experiment of pure gases. The adsorption system, including both reference and adsorption cells and pipelines connected with these cells, was first pressurized with helium gas as an inert gas (non-adsorbing gas) to measure the volume of the system. A vacuum pump was used for evacuation of the gas setup before each adsorption test. Adsorption experiments of CO_2, CH_4 and N_2 gases were done at temperature range from 298 K to 318 K and at pressure up to 14 bar.

5. Isotherm Study

One of the momentous considerations which should be noticed with respect to the large-scale application of an adsorbent is the study of isotherm models. Isotherm models enable us to estimate the equilibrium data of adsorption of the target gas over an adsorbent. Among different models formulated for isotherm study, the Sips isotherm is well-known and easily applicable [32,33].

The three-parameter Sips model provides a good description about systems with heterogeneous adsorption:

$$q = q_m \frac{bp^{1/n}}{1+bp^{1/n}} \tag{2}$$

where q_m is the maximum adsorption capacity (mmol/g), b is the Sips equilibrium constant, and n expresses the heterogeneity of adsorbent surface which could be result of the adsorbate or the adsorbent or a combination of both [34].

6. Ideal Adsorption Solution Theory (IAST)

Although, the isotherms of a pure-component adsorption system are very helpful for early understanding of the adsorbent potential in gas separation, binary isotherms data are more appropriate and valuable to appraise the adsorbent proficiency. The prediction of the adsorption amount of the single-component in a mixed-gas can be very helpful for assessment of the adsorption systems. One practical and powerful pathway to anticipate the binary adsorption systems based on the isotherms of the pure-component adsorption is ideal adsorbed solution theory (IAST), proposed by Mayer and Prausnitz [35]. In this work, the gas selectivity of binary systems (CO_2/CH_4 and CO_2/N_2) was predicted by using IAS theory and the isotherms of CH_4, N_2 and CO_2 gases. The spreading pressure (π) of a gas binary mixture (CO_2 and N_2) is determined by Eq. (3) [36]:

$$\int_0^{P^0_{CO_2}} \frac{q_{CO_2}}{P} dP = \int_0^{P^0_{CO_2}} \frac{q_{N_2}}{P} dP = \frac{\pi A}{RT} \tag{3}$$

where A is the surface area of adsorbent. Raoult's law is described below:

$$P y_{CO_2} = P^0_{CO_2} x_{CO_2} \tag{4}$$

$$y_{N_2} = P^0_{N_2} x_{N_2} \tag{5}$$

By Eqs. (4) and (5), x_i of all gases is determined. The total amount of adsorbed gas molecules can be determined from the below equation:

$$\frac{1}{q_t} = \frac{x_{CO_2}}{q_{CO_2}(P^0_{CO_2})} + \frac{x_{N_2}}{q_{N_2}(P^0_{N_2})} \tag{6}$$

where q_t and q_i (i=CO_2 and N_2) are related to the total and single-component of adsorption capacity, respectively, P^0_i is the equilibrium pressure for pure component, x_i and y_i are the mole fractions of component *i* in the adsorbed and gas phase. The selectivity of the adsorbent can be anticipated by:

$$S_{CO_2/N_2} = \frac{x_{CO_2}}{x_{N_2}} \times \frac{y_{N_2}}{y_{CO_2}} \tag{7}$$

All of the above equations are also used for the binary system of CO_2/CH_4. Instead of N_2, CH_4 is replaced.

7. Adsorption Thermodynamic

The isosteric heat of adsorption (ΔH_{st}) was applied for determining the strength of interaction between adsorbate (CO_2, CH_4 and N_2) and adsorbent (NDC) at three different temperatures. This variable is important for the design of real gas separation procedures. ΔH_{st} is calculated as follows [37]:

$$\Delta H_{st} = R \left[\frac{d \ln P}{d\left(\frac{1}{T}\right)} \right]_q \tag{8}$$

The isosteric heat of adsorption of these pure gases (CO_2, CH_4 and N_2) onto prepared NDC can be obtained by slope of isosteres (lnP versus 1/T) at different constant uptakes [38].

RESULT AND DISCUSSION

1. Physical Properties of PANI and NDC

FTIR spectra of PANI and NDC are shown in Fig. 3. For the FTIR spectrum of PANI, the peaks observed at 1,486 cm^{-1} and 1,566 cm^{-1} can be attributed to the C=C stretching vibration of benzene ring skeleton. The peak at 1,295 cm^{-1} corresponds to the C-N stretching vibration in benzenoid unit. The peak at 806 cm^{-1} is from C-H bending vibration of benzene ring. The peak located at 1,122 cm^{-1} may be due to C-N or C-O vibration. The peak at 1,655

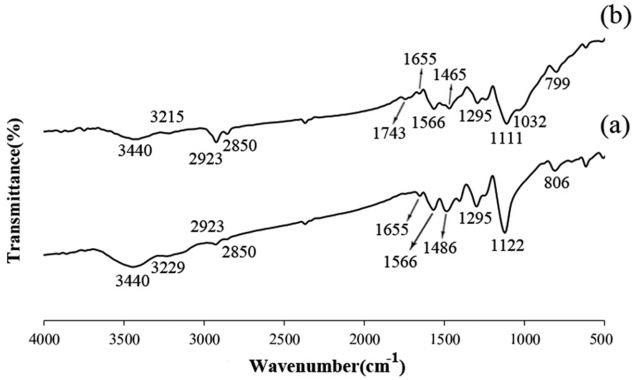

Fig. 3. FTIR spectra of PANI (a) and NDC (b).

cm^{-1} is due to the C=N groups stretching vibration of the carbon framework. The characteristic broad peaks at 3,229 cm^{-1} and 3,440 cm^{-1} correspond to the stretching vibration of N-H and O-H groups, respectively. The peaks at 2,850 cm^{-1} and 2,923 cm^{-1} are assigned to the asymmetric and symmetric stretching vibration of the -CH band [40-42]. For NDC, a new peak was observed in 1,743 cm^{-1} which can be attributed to the C=O stretching of the carbonyl groups. The emerged peaks at 1,032 cm^{-1} and 1,465 cm^{-1} are pertinent to the C-O-C and C-N stretching vibration, respectively. The peak at 3,215 cm^{-1} corresponds to the stretching vibration of N-H. The similar adsorption peaks of PANI also appeared in NDC at 1,295, 1,566, 1,655, 2,850, 2,923 and 3,440 cm^{-1}. Therefore, C-N and N-H species are present on the structure of activated carbon synthesized from the PANI.

Fig. 4 displays the SEM micrographs of the samples. The SEM image of PANI used as a carbon precursor shows granular morphology (Fig. 4(a)), which is the most typical structure in the precipitation polymerization. Such morphology is seen when PANI is synthesized in strongly acidic media [44]. After activation of PANI with KOH, large cavities and porosity were created on the surface of the NDC as shown in Fig. 4((b) and (c)). This confirms that activation with KOH agent was an effective way in forming pores on the surface of the PANI precursor.

The adsorption/desorption isotherms of N_2 and corresponding mesopore size distribution curve of prepared adsorbent are depicted in Fig. 5. The adsorption isotherm of NDC sorbent (Fig. 5(a)) exhibits a curve of type I according to the IUPAC classification due to the higher N_2 adsorption uptake in low pressure region, indicating that this adsorbent contains mainly microporous with little mesoporosity. At lower relative pressures of these isotherm, the nitrogen adsorption increases sharply with increasing pressure due to the micropore filling. At higher pressure region, pore-filling of adsorbent occurs. which causes to reach the adsorption amount to a constant value. The textural properties of the NDC are listed in Table 1. NDC prepared by KOH activation of PANI shows a relatively high specific surface area of 1,234 $m^2 \cdot g^{-1}$.

The mesopore size distribution analysis of adsorbent obtained by applying the BJH method is shown in Fig. 5(b). The pore size of NDC is close to the micropores due to the higher volume distribution near the micropore domain (1-2 nm).

The chemical composition of the PANI as a precursor and pre-

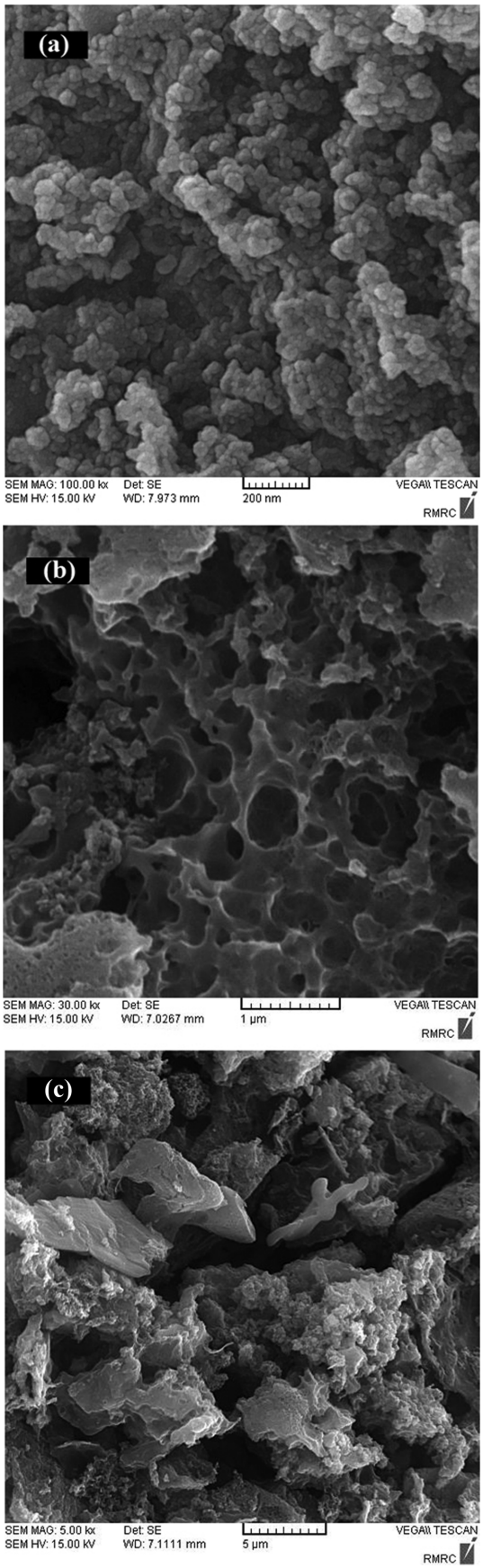

Fig. 4. SEM photographs of (a) pure polymer and NDC ((b) and (c)).

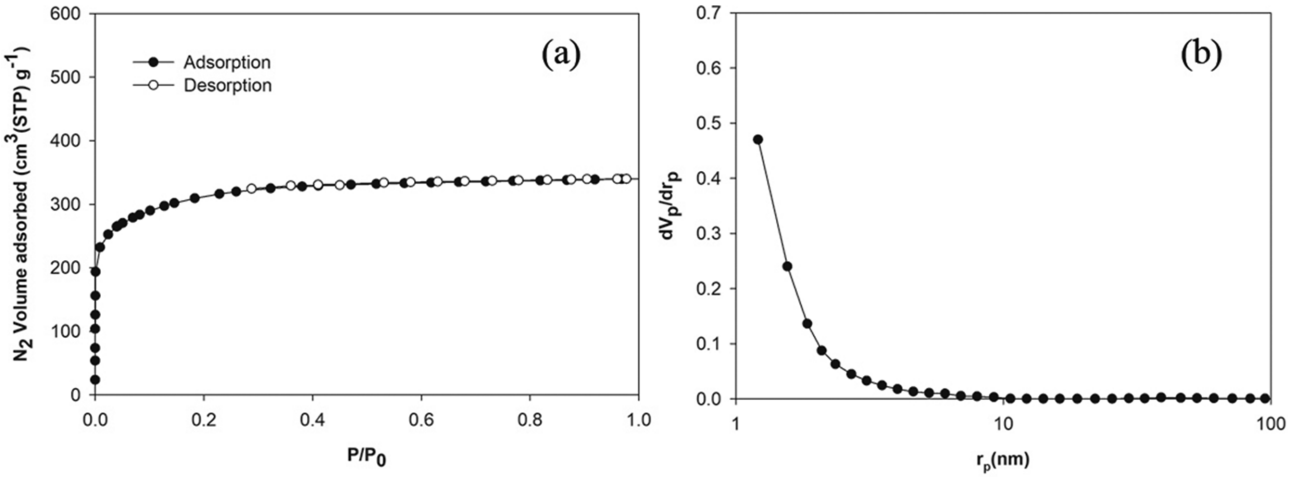

Fig. 5. (a) Adsorption-desorption isotherm of N_2 and (b) mesopore size distribution determined by BJH method for NDC.

Table 1. Textural characteristics and yield of NDC

S_{BET} (m^2/g)	1,234
V_{total} (cm^3/g)	0.58
V_{micro} (cm^3/g)	0.56
V_{meso} (cm^3/g)	0.02
d^a (nm)	1.62
Yield (%)	43.7

[a]Average pore diameter

Table 2. Ultimate analysis of PANI and NDC

Sample	Carbon	Hydrogen	Nitrogen	Sulfur	*Oxygen
PANI	53.8	5.1	11.05	4.6	25.45
NDC	56.7	2.9	8.92	0.3	31.18

*Oxygen was determined by subtracting the sum of the carbon, nitrogen, hydrogen and sulfur from 100%.

pared adsorbent from this material was determined by the CHNS analysis in Table 2. This analysis was done to investigate the level of carbon and nitrogen of precursor and prepared adsorbent. Since the carbon level plays an important role in selecting a material as a precursor, therefore PANI is suitable for preparing of adsorbent because of its high carbon content (53.8%). Another factor for choice of this material as a precursor is the relatively high level of nitrogen on it (11.05%). After carbonization process, nitrogen content of adsorbent was decreased compared to the PANI due to the elimination of nitrogenous groups. Actually, carbonization process causes to change the types of N in PANI to the pyridinic-N and this proves nitrogen doping into prepared carbon adsorbent. The presence of sulfur in PANI as well as in the synthesized adsorbent from the polymer is related to sulfuric acid. In the polymerization process, ammonium persulfate is reduced in acidic environment and this acid is not removed during the washing of the PANI and remains as a dopant in emeraldine salt form.

Increasing the amount of oxygen groups of the prepared sample indicates the introduction of oxygen from the activating agent on the adsorbent surface after activation process. According to Table 2, PANI has higher content of hydrogen and sulfur compared to the NDC because of the decomposition process of volatile materials during the carbonization process.

2. CO_2, CH_4, and N_2 Adsorption

The equilibrium adsorption capacity of gases on the NDC prepared from PANI at different temperatures (298-318 K) and pressure up to 14 bar is depicted in Fig. 6(a)-(c). In all studied temperatures, the adsorption isotherms of these pure gases are Type I adsorption isotherm based on the IUPAC scheme, which was predictable for adsorption of small gas molecules on a microporous material. For CH_4 and N_2, the critical temperature was lower than the experimental temperature (190.6 K and 126.2 K, respectively); therefore, the mechanism of adsorption of these gases is monolayer supercritical adsorption. But, due to the closing of the CO_2 critical temperature (304.1 K) with the experimental temperature range, the CO_2 adsorption process by NDC involved supercritical adsorption and subcritical adsorption. Therefore, in this study the adsorption isotherm was of the type I due to the filling of micropores (less than 2 nm in size) at subcritical temperature [47]. With decrement in temperature, the amount of adsorption for all gases was reduced, indicating the exothermal nature of adsorption reaction of these gases with NDC. Among the studied gases under similar process conditions (temperature and pressure), the quantity of CO_2 adsorbed onto NDC was significantly higher than the amount of CH_4 and N_2 adsorbed on the NDC and increased rapidly at lower pressure relative to the other gases. Therefore, there is a different adsorption mechanism between NDC and these three gases. Actually, due to the higher value of CO_2 adsorption, there is a great affinity between CO_2 molecules and NDC adsorbent, especially at low pressures.

One of the reasons for this is the existence of nitrogen groups on the NDC surface, which causes to increase the selectivity of CO_2 molecules as an acidic gas with adsorbent. Therefore, strong pole-pole interactions are created between the large electrostatic quadrupole moment of CO_2 molecules and the polar sites of nitrogen groups in the NDC. Based on Table 3, compared to the CH_4 and N_2, CO_2 has larger quadrupole moment and polarization.

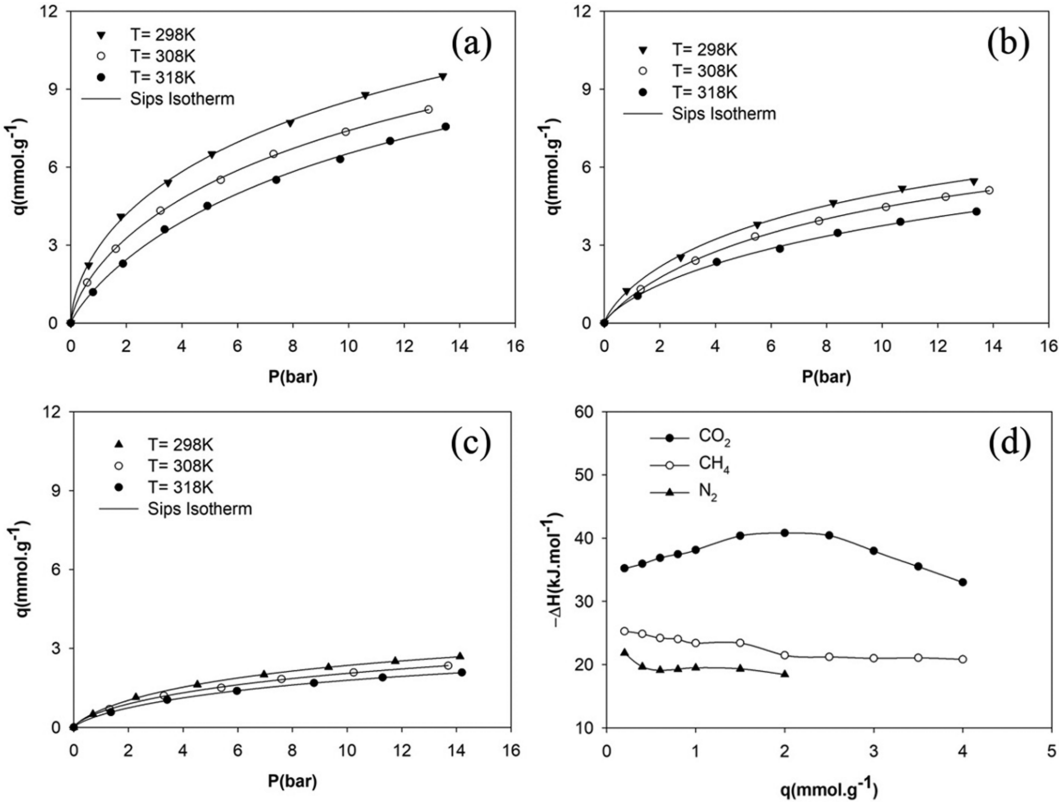

Fig. 6. Adsorption isotherms and curve fitting of these experimental data with Sips isotherm model for CO_2 (a), CH_4 (b) and N_2 (c) and the alteration of ΔHst versus surface loading (d).

Table 3. Physical properties of the CO_2, CH_4 and N_2 [48,49]

	Molecular weight, M (g/mol)	Critical temperature, T_c (K)	Permanent electric dipolar moment, μ_e (Debye)	Polarizability	Quadrupole moment, q_m (esu/cm^2)	Kinetic diameter, d_k (nm)
CO_2	44	304.1	0	$29.1*10^{-25}$	$4.3*10^{-26}$	0.33
CH_4	16	190.6	0	$25.9*10^{-25}$	0	0.38
N_2	28	126.2	0	$17.6*10^{-25}$	$1.52*10^{-26}$	0.36

Hence CO_2 as the acidic molecule displays stronger interaction with polar interpole of the nitrogen group of NDC rather than CH_4 and N_2 [46]. Another reason is related to the molecular sieve effect of NDC. In transport phenomena, the kinetic diameter of a gas is considered as the ability of a gas molecule for moving in highly restrictive environment. Therefore, the molecule of gas with the smallest kinetic diameter diffuses faster through the pores. According to Table 3, CH_4 (0.38 nm) and N_2 (0.36 nm) have larger kinetic diameter than CO_2 (0.33 nm), which causes to diffuse CO_2 molecules through the ultramicropores in NDC while remaining inaccessible for N_2 and CH_4. The third reason for higher CO_2 adsorption is somehow due to the O groups in the NDC surface (Table 1). Since partial pressure of CO_2 is low in flue gas, the O groups provide sufficient active CO_2-adsrobing sites to capture acidic guest molecules [45]. Therefore, the presence of O groups in the NDC (by KOH) seems to be promising for capture of CO_2 from flue gas. It is clear that the amount of CH_4 adsorbed on the NDC was higher than N_2, which is attributed to the higher polarizability of CH_4 than N_2 (Table 3) despite its non-polar nature. This caused to create stronger interactions between molecules of CH_4 with NDC com-

Table 4. The parameters of fitted isotherm model for pure gases

Gas	Temperature (K)	Sips model			
		q_m (mmol/g)	b	n	R^2
CO_2	298	22.4	0.150	1.630	0.999
	308	18.7	0.129	1.423	1.000
	318	15.3	0.105	1.279	0.996
CH_4	298	11.3	0.144	1.366	0.999
	308	10.8	0.118	1.292	1.000
	318	10.3	0.096	1.199	0.999
N_2	298	6.08	0.136	1.342	1.000
	308	5.64	0.116	1.282	1.000
	318	4.26	0.090	1.121	1.000

pared to N_2 molecules. N_2 molecules have lower polarizability and a weak quadrupole moment. The amount of CO_2, CH_4 and N_2 adsorption by NDC was obtained as 3.09, 1.43 and 0.64 $mmol \cdot g^{-1}$ at 298 K and 1 bar, respectively.

The single-component adsorption isotherms of all three gases measured at 298, 308 and 318 K were fitted by the Sips isotherm model (Fig. 6(a)-(c)). According to the correlation coefficients (R^2) obtained from the Sips model (Table 4), it is obvious that in the pressure range studied, this model well fitted with experimental data. The maximum adsorption amount (q_{max}) obtained from this model, for CO_2, CH_4 and N_2 gases, has had a decreasing trend with temperature indicating the exothermic adsorption of these gases on the NDC. Also, the amount of this parameter for CO_2 was about more than twice of CH_4 and more than three times of N_2, which confirms good affinity between CO_2 and NDC compared to the other gases studied in this work. As mentioned earlier, the n parameter in Sips isotherm model represents the heterogeneity degree of the system and shows the steepness of the isotherm at low pressure range. With decreasing n value, the adsorption proceeds much slower. From Table 4, with the temperature increasing, a decrease of the values of n (as a heterogeneity factor) and b (as an affinity constant) for all gases was observed. For CO_2, these two parameters were higher than CH_4 and N_2, which revealed that there is a stronger affinity between the surface of prepared NDC and CO_2

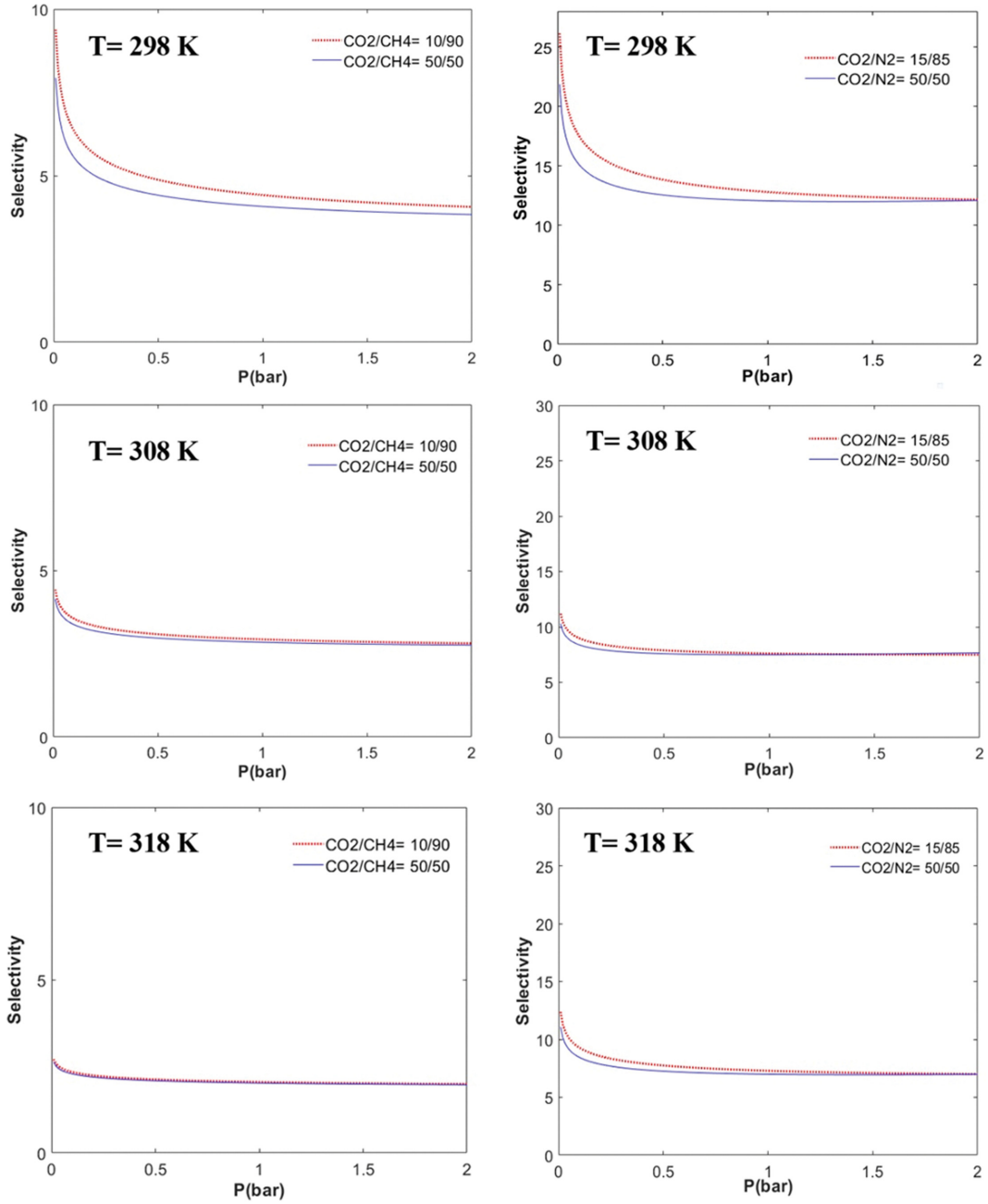

Fig. 7. Adsorption selectivity as a function of total pressure at different temperatures.

molecules rather than CH_4 and N_2.

3. Selectivity

As mentioned, the adsorption isotherms of CO_2, CH_4 and N_2 at different temperatures were well fitted with Sips isotherm model. The molar ratio of CO_2/N_2 in flue gas streams and CO_2/CH_4 in natural gas is close to 15/85 and 10/90, respectively. Therefore, in this study, selectivities of CO_2/N_2 (50/50 and 15/85, v/v) and CO_2/CH_4 (50/50 and 10/90, v/v) over prepared NDC were calculated. Fig. 7 shows the adsorption selectivity as a function of total pressure at different temperature. For all temperatures and different gas mixtures, the selectivity of CO_2 over CH_4 and N_2 is higher at lower pressure and then decreases with increasing total pressure due to favorable binding interactions between CO_2 molecules and nitrogen sites on the surface of the NDC at lower pressure. With increasing surface loading, these sites become occupied, resulting in more competition between the mixture species due to the dominance of the van der Waals interactions on the adsorption behavior. It is observed from Fig. 7 that in pressure region (up to 2 bar), selectivity of CO_2/CH_4=10/90 mixture in all three temperatures was higher than that for CO_2/CH_4=50/50 mixture. Similar trend was observed for selectivity of CO_2/N_2=15/85 mixture rather than CO_2/N_2=50/50 mixture. This increase is because of the strong adsorption sites in the NDC structure and saturation of these sites in lower concentration of CO_2 in CO_2/CH_4=10/90 and CO_2/N_2=15/85 compared to the volume fraction of v/v=50/50. The adsorption selectivity values for the two gas mixtures at different compositions are shown in Table 5 at 298-318 K and 1 bar. With increasing temperature, CO_2/CH_4 and CO_2/N_2 selectivity was decreased. Therefore, there is greater potential at lower temperature for the separation of CO_2 from CH_4 and N_2. Also, as shown in Fig. 7 and Table 5, it seems that the effect of the composition of gases on selectivity decreases with increasing temperature. The selectivity of CO_2/N_2= 15/85 mixture of this adsorbent prepared in this study (IR=2, T= 650 °C, t=1 h) is more than two-times higher than the selectivity of our previous work (IR=1, T=650 °C, t=1 h) [27].

4. Heat of Adsorption

Further information about CO_2, CH_4 and N_2 adsorption mechanisms with this prepared adsorbent was obtained by determination of the isosteric heat of adsorption (ΔH_{st}). Fig. 6(d) shows the variation of ΔH_{as} with the surface loading. The negative change of enthalpy for all gases used in this work confirms that the adsorption process by prepared sorbent had exothermic nature. In all studied surface loading, the isosteric heat of adsorption of CO_2 was significantly larger than CH_4 and N_2 gases and reached about to 41 kJ/mol. In addition, the isosteric heat of CO_2 follows a different trend compared to the CH_4 and N_2. With increasing of CO_2 loading from 0.2 to 2 mmol/g, the ΔH_{st} of CO_2 increased from about 35 kJ/mol to 41 kJ/mol. This is due to the existence of strong adsorption sites in the NDC sorbent and gradual occupation of these sites with increasing surface coverage. Actually, in CO_2 adsorption and at the adsorption process beginning, strong binding sites are available and will first be occupied by CO_2 molecules and weak binding sites become unoccupied and available. Higher value of the isosteric heat of CO_2 verifies the presence of strong interaction between CO_2 molecules and the NDC surface. This interaction involves the van der Waals force and the weak chemical interaction between basic nitrogen groups in the NDC structure and acidic CO_2 molecules. Therefore, there is a physico-chemical adsorption process by this synthesized adsorbent rather than absolute physical or chemical adsorption phenomena. Note that the isosteric heat of CO_2 by this adsorbent is moderate (not too high) from the viewpoint of potential applications such as flue gas separation [50]. Upon increasing CO_2 loadings from 2 to 4 mmol/g, the ΔH_{st} of CO_2 was decreased. This reduction at higher surface coverages occurred for two reasons. First is the occupation of sites with less-active adsorption. Because with increasing the equilibrium surface loading, further chemical reaction between nitrogen functional groups and CO_2 molecules becomes more difficult. The second reason is due to the adsorbate-adsorbate interaction between the adsorbed CO_2 molecules. Therefore, the adsorption enthalpy (ΔH_{st}) of CO_2 over the entire range of gas uptake was non-uniform, indicating that the surface of the NDC for CO_2 is heterogeneous.

The adsorption enthalpy of CH_4 and N_2 displays initially a slight decreasing trend at lower surface loading, indicating the energetic heterogeneity of the NDC surface for CH_4 and N_2 gases. At higher surface coverage, ΔH_{st} is almost constant and independent of the surface loading, ascribed to a balance between the strength of cooperative gas-gas interactions and the degree of heterogeneity of gas-solid interactions [51]. The heat of adsorption obtained in this study had suitable values, which confirms that this sorbent is a promising candidate in the gas separation process.

Table 5. Adsorption selectivity of CO_2/CH_4 and CH_4/N_2 at pressure of 1 bar

T (K)	Selectivity of CO_2/CH_4		Selectivity of CO_2/N_2	
	(10/90, v/v)	(50/50, v/v)	(15/85, v/v)	(50/50, v/v)
298	4.42	4.08	12.81	12.07
308	2.93	2.85	7.60	7.48
318	2.05	2.02	7.29	6.99

CONCLUSION

Porous nitrogen-doped activated carbon (NDC) was fabricated from PANI as a nitrogen-containing precursor by chemical activation with KOH, and adsorption amount of three gases (CO_2, CH_4 and N_2) was determined at different temperatures. The amount of pure gas adsorption by NDC was obtained 3.09, 1.43 and 0.64 $mmol \cdot g^{-1}$ at 298 K and 1bar for CO_2, CH_4 and N_2, respectively. According to the R^2 value, Sips model was suitable for describing the adsorption isotherm of all gases studied in this work, indicating multilayer gas adsorption and heterogeneous surface binding. The calculated maximum adsorption capacity predicted by the Sips model was obtained 22.4, 11.3 and 6.08 mmol/g for CO_2, CH_4 and N_2, respectively, at 298 K. The selectivity of CO_2 over CH_4 and N_2 by NDC obtained from the ideal adsorbed solution theory (IAST) was mainly affected by temperature and gas mixture. The best selectivity of CO_2/N_2 and CO_2/CH_4 was obtained at lower temperature (298 K) and lower CO_2 concentration, which was 12.81 and 4.42 for CO_2/N_2=15/85 and CO_2/CH_4=10/90 at pressure of 1 bar. In all studied surface loadings, the isosteric heat of adsorption of CO_2

(33-41 kJ/mol) was significantly larger than CH_4 (21-25 kJ/mol) and N_2 (18-21 kJ/mol) gases, indicating the presence of strong interaction between CO_2 molecules and the NDC surface. Actually, both physical adsorption (adsorption of CO_2 in the pores of NDC) and chemical adsorption (interaction of CO_2 molecules with nitrogen groups in the NDC structure) occurred in CO_2 adsorption. Whereas, it seems only physical adsorption happened in CH_4 and N_2 adsorption by NDC. The obtained results in this study confirm that this sorbent is a promising candidate in gas separation process such as natural gas and flue gas processing.

ACKNOWLEDGEMENT

The authors acknowledge the funding support of Babol Noshirvani University of Technology through Grant program No. BNUT/370302/98.

REFERENCES

1. Y. Li, R. Xu, B. Wang, J. Wei, L. Wang, M. Shen and J. Yang, *Nanomaterials*, **9**, 266 (2019).
2. A. Modak and A. Bhaumik, *J. Solid State Chem.*, **232**, 157 (2015).
3. S. Vasudevan, S. Farooq, I. A. Karimi, M. Saeys, M. C. Quah and R. Agrawal, *Energy*, **103**, 709 (2016).
4. D. Lv, J. Chen, K. Yang, H. Wu, Y. Chen, C. Duan, Y. Wu, J. Xiao, H. Xi and Z. Li, *Chem. Eng. J.*, **375**, 122074 (2019).
5. S. Xian, J. Peng, Z. Zhang, Q. Xia, H. Wang and Z. Li, *Chem. Eng. J.*, **270**, 385 (2015).
6. H. S. Kim, M. S. Kang, S. Lee, Y.-W. Lee and W. C. Yoo, *Micropor. Mesopor. Mater.*, **272**, 92 (2018).
7. M. Hoorfar, Y. Alcheikhhamdon and B. Chen, *Comput. Chem. Eng.*, **117**, 11 (2018).
8. M. Zia-ul-Mustafa, H. Mukhtar, N. Nordin and H. Mannan, *Mater. Today. Proc.*, **16**, 1976 (2019).
9. C. Song, Q. Liu, S. Deng, H. Li and Y. Kitamura, *Renew. Sust. Energy Rev.*, **101**, 265 (2019).
10. W.-T. Zheng, K. Huang and S. Dai, *Micropor. Mesopor. Mater.*, **290**, 109653 (2019).
11. H.-L. Peng, J.-B. Zhang, J.-Y. Zhang, F.-Y. Zhong, P.-K. Wu, K. Huang, J.-P. Fan and F. Liu, *Chem. Eng. J.*, **359**, 1159 (2019).
12. B. Chang, W. Shi, H. Yin, S. Zhang and B. Yang, *Chem. Eng. J.*, **358**, 1507 (2019).
13. S. S. Fiyadh, M. A. AlSaadi, W. Z. Jaafar, M. K. AlOmar, S. S. Fayaed, N. S Mohd, L. S. Hin and A. El-Shafie, *J. Clean. Prod.*, **230**, 783 (2019).
14. M. Xu, S. Chen, D.-K. Seo and S. Deng, *Chem. Eng. J.*, **371**, 693 (2019).
15. S. Jribi, T. Miyazaki, B. B. Saha, A. Pal, M. M. Younes, S. Koyama and A. Maalej, *Int. J. Heat Mass Transfer*, **108**, 1941 (2017).
16. X. Weng, Y. Cui, S. Shaikhutdinov and H.-J. Freund, *J. Phys. Chem. C*, **123**, 1880 (2018).
17. G. Gómez-Pozuelo, E. Sanz-Pérez, A. Arencibia, P. Pizarro, R. Sanz and D. Serrano, *Micropor. Mesopor. Mater.*, **282**, 38 (2019).
18. R. Kishor and A. K. Ghoshal, *Chem. Eng. J.*, **262**, 882 (2015).
19. J. Wang, R. Krishna, X. Wu, Y. Sun and S. Deng, *Langmuir*, **31**, 9845 (2015).
20. L. An, S. Liu, L. Wang, J. Wu, Z. Wu, C. Ma, Q. Yu and X. Hu, *Ind. Eng. Chem. Res.*, **58**, 3349 (2019).
21. P. Nugent, Y. Belmabkhout, S. D. Burd, A. J. Cairns, R. Luebke, K. Forrest, T. Pham, S. Ma, B. Space and L. Wojtas, *Nature*, **495**, 80 (2013).
22. R. Zhong, Z. Xu, W. Bi, S. Han, X. Yu and R. Zou, *Inorg. Chim. Acta*, **443**, 299 (2016).
23. M. Kacem, M. Pellerano and A. Delebarre, *Fuel Process. Technol.*, **138**, 271 (2015).
24. S. Khalili, B. Khoshandam and M. Jahanshahi, *RSC Adv.*, **6**, 35692 (2016).
25. J. Singh, S. Basu and H. Bhunia, *Micropor. Mesopor. Mater.*, **280**, 357 (2019).
26. A. C. Dassanayake and M. Jaroniec, *Colloids Surf. A Physicochem. Eng. Asp.*, **549**, 147 (2018).
27. E. Qezelsefloo, S. Khalili, M. Jahanshahi and M. Peyravi, *Mater. Chem. Phys.*, **239**, 122304 (2020).
28. X. Li, Z.-Y. Sui, Y.-N. Sun, P.-W. Xiao, X.-Y. Wang and B.-H. Han, *Micropor. Mesopor. Mater.*, **257**, 85 (2018).
29. J. Pallarés, A. González-Cencerrado and I. Arauzo, *Biomass Bioenergy*, **115**, 64 (2018).
30. E. Apaydın-Varol and Y. Erülken, *J. Taiwan Inst. Chem. Eng.*, **54**, 37 (2015).
31. J. Singh, S. Basu and H. Bhunia, *Micropor. Mesopor. Mater.*, **280**, 357 (2019).
32. S. Khalili, B. Khoshandam and M. Jahanshahi, *RSC Adv.*, **6**, 35692 (2016).
33. P. Ammendola, F. Raganati and R. Chirone, *Chem. Eng. J.*, **322**, 302 (2017).
34. F. Raganati, M. Alfe, V. Gargiulo, R. Chirone and P. Ammendola, *Chem. Eng. Res. Des.*, **134**, 540 (2018).
35. A. L. Myers and J. M. Prausnitz, *AIChE J.*, **11**, 121 (1965).
36. D. D. Do, *Adsorption analysis: Equilibria and kinetics (with cd containing computer MATLAB programs)*, World Scientific, London (1998).
37. V. Garshasbi, M. Jahangiri and M. Anbia, *Appl. Surf. Sci.*, **393**, 225 (2017).
38. S. Zohdi, M. Anbia and S. Salehi, *Polyhedron*, **166**, 175 (2019).
39. A. Heidari, H. Younesi, A. Rashidi and A. A. Ghoreyshi, *Chem. Eng. J.*, **254**, 503 (2014).
40. Y. Huangfu, K. Ruan, H. Qiu, Y. Lu, C. Liang, J. Kong and J. Gu, *Compos. Part A Appl. Sci. Manuf.*, **121**, 265 (2019).
41. S. Daikh, F. Zeggai, A. Bellil and A. Benyoucef, *J. Phys. Chem. Solids*, **121**, 78 (2018).
42. V. Janaki, K. Vijayaraghavan, B.-T. Oh, K.-J. Lee, K. Muthuchelian, A. Ramasamy and S. Kamala-Kannan, *Carbohydr. Polym.*, **90**, 1437 (2012).
43. M. A. Tofighy and T. Mohammadi, *Chem. Eng. Res. Des.*, **90**, 1815 (2012).
44. J. Stejskal, I. Sapurina and M. Trchová, *Prog. Polym. Sci.*, **35**, 1420 (2010).
45. J. Wang, R. Krishna, X. Wu, Y. Sun and S. Deng, *Langmuir*, **31**, 9845 (2015).
46. J. Park, N. F. Attia, M. Jung, M. E. Lee, K. Lee, J. Chung and H. Oh, *Energy*, **158**, 9 (2018).
47. W. Su, L. Yao, M. Ran, Y. Sun, J. Liu and X. Wang, *J. Chem. Eng.*

Data, **63**, 2914 (2018).
48. S. Y. Sawant, R. S. Somani, H. C. Bajaj and S. S. Sharma, *J. Hazard. Mater.*, **227**, 317 (2012).
49. P. S. Bárcia, L. Bastin, E. J. Hurtado, J. A. Silva, A. E. Rodrigues and B. Chen, *Sep. Sci. Technol.*, **43**, 3494 (2008).
50. L. Wang, L. Rao, B. Xia, L. Wang, L. Yue, Y. Liang, H. DaCosta and X. Hu, *Carbon*, **130**, 31 (2018).
51. N. Álvarez-Gutiérrez, M. Gil, F. Rubiera and C. Pevida, *Fuel Process. Technol.*, **142**, 361 (2016).